

ARTICLE

Simulation of Deep Water Wave Climate for the Indian Seas

J. Swain¹ P. A. Umesh^{1,2*} M. Baba³ A. S. N. Murty⁴

1. Naval Physical & Oceanographic Laboratory, Cochin, 682021, India

2. Department of Physical Oceanography, Cochin University of Science and Technology, Cochin, 682016, India

3. National Centre for Earth Science Studies, Thiruvananthapuram, 695011, India

4. Department of Marine Science, Berhampur University, Berhampur, 761007, India

ARTICLE INFO

Article history

Received: 23 April 2021

Accepted: 11 May 2021

Published Online: 13 May 2021

Keywords:

3g-WAM

Wave climate simulation

Wave model validation

Mean climatic year of winds

ABSTRACT

The ocean wave climate has a variety of applications in Naval defence. However, a long-term and reliable wave climate for the Indian Seas (The Arabian Sea and The Bay of Bengal) over a desired grid resolution could not be established so far due to several constraints. In this study, an attempt was made for the simulation of wave climate for the Indian Seas using the third-generation wave model (3g-WAM) developed by WAMDI group. The 3g-WAM as such was implemented at NPOL for research applications. The specific importance of this investigation was that, the model utilized a “mean climatic year of winds” estimated using historical wind measurements following statistical and probabilistic approaches as the winds which were considered for this purpose were widely scattered in space and time. Model computations were carried out only for the deep waters with current refraction. The gridded outputs of various wave parameters were stored at each grid point and the spectral outputs were stored at selected locations. Monthly, seasonal and annual distributions of significant wave parameters were obtained by post-processing some of the model outputs. A qualitative validation of simulated wave height and period parameters were also carried out by comparing with the observed data. The study revealed that the results of the wave climate simulation were quite promising and they can be utilized for various operational and ocean engineering applications. Therefore, this study will be a useful reference/demonstration for conducting such experiments in the areas where wind as well as wave measurements are insufficient.

1. Introduction

The ocean wave climate refers to the general condition or the sea-state of a specific location or over a coastal or offshore region. The principal elements that are associated with wave climate are the significant wave parameters such as significant wave height (Hs), significant wave pe-

riod (Ts) and direction. As in the atmospheric climate, the wave climate is generally described in terms of months, seasons, and years. The fundamental requirements for the generation of a suitable wave climate of any given region are quality and duration of the wave data acquired from one or more sources. The type of data which can be utilized for the establishment of wave climate are visually

*Corresponding Author:

P. A. Umesh,

Naval Physical & Oceanographic Laboratory, Cochin, 682021, India; Department of Physical Oceanography, Cochin University of Science and Technology, Cochin, 682016, India;

Email: umeshpa.nair@gmail.com

observed data, instrumentally/ satellite measured wave data, hindcast wave data and operational wave forecast data. Visually observed wave data usually involve a significant degree of estimation variability. Measured wave data using state-of-the-art equipment are most reliable but there are limited deep water measurements available in the Arabian Sea and Bay of Bengal (hereinafter referred to as the Indian Seas). Earlier, the main source of long-term winds available from India Meteorological Department (IMD) for wave hindcasting in the Indian Seas was the daily weather reports/charts. However, there use to be limited wind as well as barotropic (atmospheric pressure) data which were used for the preparation of Indian Daily Weather Reports (IDWR). As the atmospheric pressure is more accurately measured compared to winds, wind fields are usually estimated based on the pressure values. However, if the available measurements are limited, the estimation of winds for the whole of the Indian Seas (over 1 x 1 degree grids) based on these synoptic charts will have greater uncertainty. For a long-term wave hindcast, winds should be preferably estimated at regular intervals of, say, 3 or 6 hours. If the wind input to the wave model has a bias, the hindcast based on these estimates will have further bias^[1]. In this study, an attempt was made to simulate the wave climate for the Indian Seas based on the estimated “mean climatic year of winds” using the available instantaneous wind measurements from various sources.

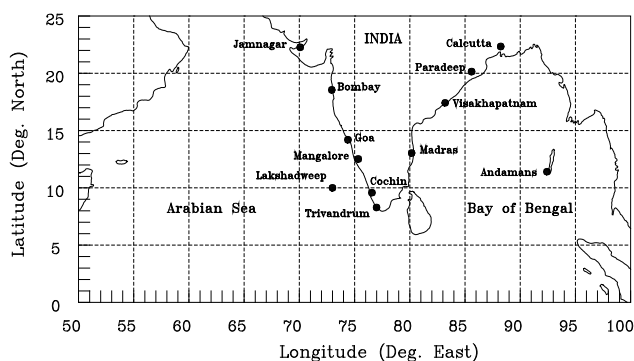


Figure 1. Map showing Indian Seas, the area of study.

In the absence of a high resolution, reliable and up-to-date wave climate or wave database for the Indian Seas, long-term simulation/prediction appeared to be the best and only alternative^[2, 3]. The present simulation experiment was planned for the seas around India (Figure 1) which extend from 50° to 100° E and 0° to 25° N. India has a long coast line of about 7000 Km bordering the Arabian Sea (West coast) and Bay of Bengal (East Coast). The assumed boundary in the present study separating the Arabian Sea and Bay of Bengal is the 80 degree longitude. The area covered in this study has only one open sea boundary

to the south (0° latitude). The other three sides are almost enclosed by land. Wave conditions which prevail in this region showed both temporal and spatial variability along with the wind and it was important to study and provide support both for civilian and defence applications^[4, 5]. Although, the wave data available for this region were limited, we had some qualitative picture and long-term understanding of the problem/variability addressed here. In this study, suitable attempts were made for a clear understanding and quantification of the same from a climatic point of view. Therefore, long-term winds representing a mean climatic year and the monthly mean surface current fields were utilized as the inputs. The wave model outputs were processed over 1x1 degree resolution and the same were the basis for establishment of wave climate of this region considered based on model simulations.

2. Selection of Wave Model

Selection of a model is an important task while dealing with the problem of wave climate simulation. In the past, several empirical/climatological models were used to hindcast/predict wave climate/conditions using hourly/six-hourly values of wind inputs by various researchers and some of them are available as the useful references for wave researchers in India^[6, 3,7]. These models are termed as wave climate models. They use a pragmatic back stepping procedure to handle varying wind speed from a constant direction but the treatment of variation in wind direction is too complex^[8]. The averaging procedure for input wind speed is continued as long as the wind direction remains within a practicable range and the duration of average does not exceed a prescribed limit. These problems are not encountered if one uses a numerical wave model by neglecting the computational economy offered by the empirical models. Empirical models normally compute the significant wave parameters of the regions for which the winds are assumed to be more or less uniform while the present day numerical models are capable of providing two dimensional wave spectra at each grid point of the model. Moreover, this task being a simulation experiment, it involved a special procedure for specifying the wind input which is not similar to hindcast methods. Therefore, the use of an empirical model in this case could not yield the expected results. From these considerations, the third generation wave model 3g-WAM^[9,10] appeared to be the most appropriate in this study, because it is capable of simulating wave fields for a variety of wind conditions^[11]. The model provided the gridded outputs of various wave parameters at selected time steps. However, the two dimensional spectral outputs were available only for selected grids and time steps. The list of all the model outputs which were saved

during the simulation is given below:

- I. Significant wave height
- II. Mean wave direction
- III. Mean wave frequency
- IV. Friction wind speed
- V. Friction wind direction
- VI. Peak wave frequency
- VII. Sea-state dependent drag coefficient
- VIII. Normalized wave stress
- IX. Swell wave height
- X. Mean swell direction
- XI. Mean sea direction
- XII. Mean swell frequency
- XIII. 2-dimensional wave spectra
- XIV. 2-dimensional swell spectra

3. Input Data for Wave Climate Simulation

Past IDWR wind data from 1961 to 1970 were obtained from IMD, New Delhi and utilized in the present study. As sufficient and more accurate data are presently available from various sources including satellite measurements, this investigation is only a demonstration of wave climate simulation to its readers which is further explained in detail. Figure 2a shows the wind data distribution for the Indian Seas (IMD, 1961-70) over one degree square grids. The mean monthly wind fields of Indian Seas published in the “Climatic atlas of the Indian Ocean, Part-I: Surface climate and atmospheric circulation” by Hastenrath and Lamb (H & L) (1979)^[12] was also utilized in this study. The above indicated digital wind data of Hastenrath and Lamb (1979)^[12] used in this investigation was obtained from the Department of Atmospheric and Oceanic Sciences, University of Wisconsin, Madison, U.S.A. The monthly estimates of this atlas over one-degree grid resolution were computed based on the observations made by ships for a period of sixty years^[12]. Surface current data distribution as shown in Figure 2b were mostly based on the ship drift measurements from 1954 to 1994. These current data were obtained from the Meteorological Office, Berkshire, U.K. in the form of monthly means for two degree square grids. The size of the thick circle for a given grid indicates the number of observations corresponding to one particular range as indicated on top of the above mentioned figure. It may be noticed that, the wind as well as surface current data was concentrated along shipping lanes. The mean monthly variations of wind in space and time were established based on the above mentioned data sets covering 10 to 60 years. A detailed account of the wind (IMD) and surface current data strength for the individual months is given in Table 1 below.

Table 1. Number of data points used for the preparation and analysis of wave model input data.

Sl. No.	Month	Wind Surface Current	
		1961-70	1954-94
1	January	51,587	36,149
2	February	53,466	27,969
3	March	57,974	37,898
4	April	54,424	28,556
5	May	56,726	32,664
6	June	54,394	30,260
7	July	55,162	29,794
8	August	56,679	30,236
9	September	50,603	32,149
10	October	53,093	28,671
11	November	51,343	28,883
12	December	51,683	30,035
TOTAL		6,47,136	3,73,264

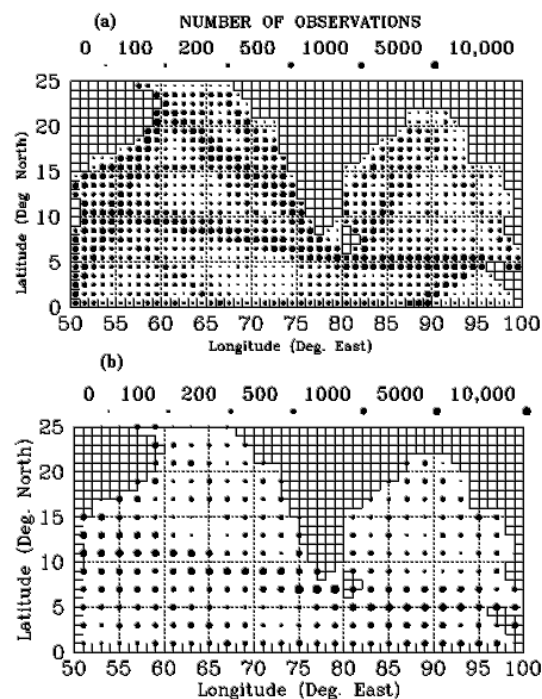


Figure 2. Input data distribution for Indian Seas: [a] Winds 1961-70 and, [b] Surface currents 1954-94 (The size of the thick circle for a given grid indicates the number of observations corresponding to one particular range as indicated on top of the figures).

3.1 Estimation of Mean Monthly Wind Fields

As the IMD wind data (1961-70) density is much higher compared to that of H&L (1911-70^[12]), both the data sets were suitably combined to estimate the resultant wind fields (weighted averages based on number of data points). The mean winds using IMD data was computed as given below.

$$\bar{X}_0 = \frac{\sum_{i=1961}^{1970} N_i X_i}{\sum_{i=1961}^{1970} N_i} \quad (1)$$

where *i* denotes the year, *X* denotes individual monthly mean value of a given parameter, *N* denotes the number of observations from which individual monthly means were computed and \bar{X}_{10} is the calculated ten-year average of the parameter considered (in this case, *u* or *v* component of wind).

The *u* and *v* components are computed using the ship reported wind speed (*U* in m/s) and direction (*θ* in degrees) using the following equation:

$$\begin{aligned} u &= U \cdot \cos\theta \\ v &= U \cdot \sin\theta \end{aligned} \quad (2)$$

While computing the above mentioned individual mean monthly wind components for different years, a simple two way interpolation scheme^[13] is adopted for the grids without any observation. Finally, the ten-year mean components over one degree resolution were smoothed using Laplacian method^[14]. It is ascertained that only a part of the IMD wind data (less than 30%) has formed the basis of the sixty-year mean wind fields of Hastenrath and Lamb (1979)^[12]. Therefore, the ten-year average of IMD data (\bar{X}_{10}) and the sixty-year average of H & L (\bar{X}_{60}) are combined as follows:

$$\bar{X}_{60} = \frac{6.0(\bar{X}_{60}) + 0.7(\bar{X}_{10})}{6.0 + 0.7} \quad (3)$$

where \bar{X}_{10} is the combined wind component of the sixty-year mean and the ten-year mean wind components (with 6.0 and 0.7 weightages respectively) as shown in the above equation. Finally, the resultant wind speed and direction for the individual months over a one-degree grid were estimated as follows:

$$\begin{aligned} WS &= \sqrt{u^2 + v^2} \\ WD &= \tan^{-1} \left[\frac{u}{v} \right] \end{aligned} \quad (4)$$

Following equations (1) to (4), the monthly wind fields for the Indian Seas from January to December averaged over one degree squares were estimated and shown in Figure 3 for two representative months. The contours

represent wind speed in meters/second and the arrows represent wind direction from true north. Figure 4 shows the observed joint probability distributions of wind components in the Arabian Sea and Bay of Bengal for January and July respectively. The general pattern of wind variations is clearly depicted in these distributions. Similar distributions are computed for the individual model grids through objective analysis as the data strength is limited for the grids outside the shipping lanes.

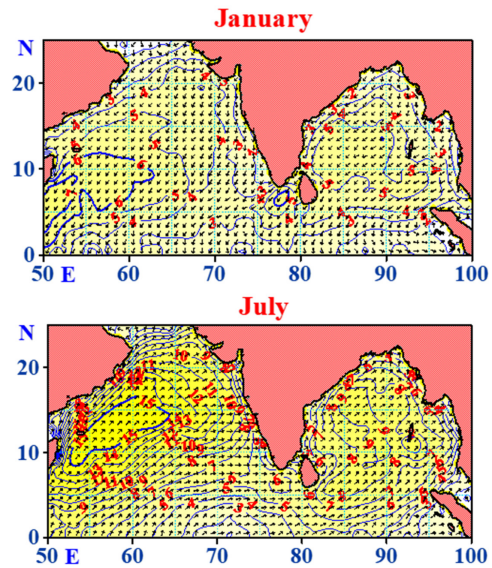


Figure 3. Mean monthly surface wind fields for January and July (contour interval 1m/s).

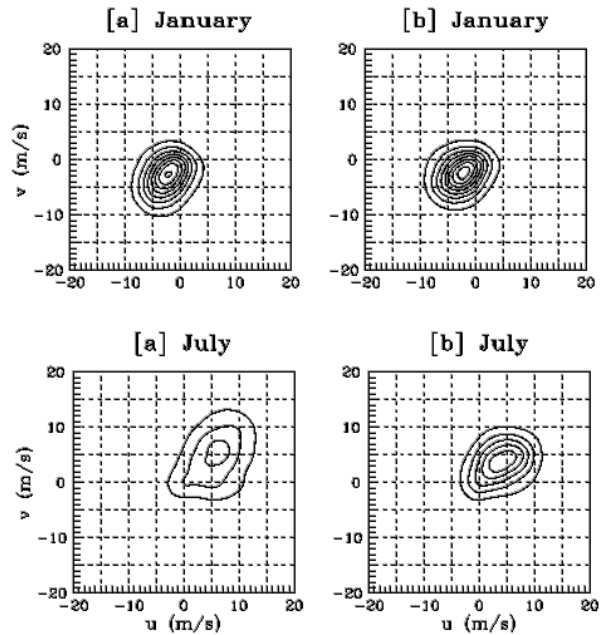


Figure 4. Observed joint probability distribution for *u* and *v* components of wind [a] Arabian Sea, [b] Bay of Bengal. Values of lowest contour (outermost) and contour interval are 0.002.

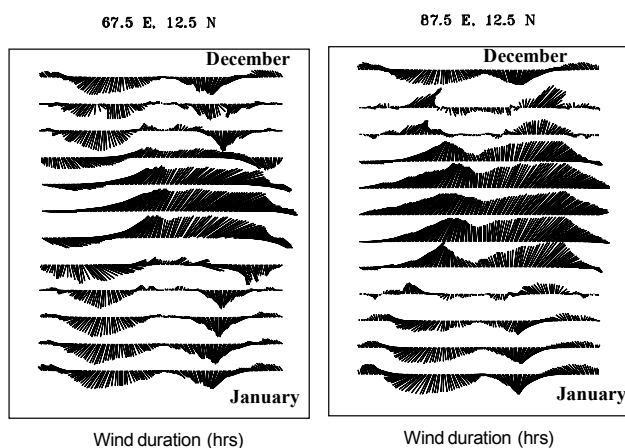


Figure 8. Mean climatic year of winds for two selected locations (grid positions given on top of each plot).

However, the number of observations could reach close to 600 only for a few grids during some of the months. Hence, the data from neighbouring grids were considered to attain the required number of observations. The schematic diagram shows (Figure 7) the search radius for the grids which did not satisfy the above condition for the month of January. As an example, if the search radius was 1, equal number of observations from each of the adjacent grids distributed over a ten-year period (by selecting a suitable time window required) were used to cater for the observations in short of 600. The total number of grids considered in this case was nine (3x3). For a search radius of 2, data from 25 grids including the representative grid were considered, and so on. Search radii for the other months were also estimated for analysis.

Figure 6 indicate that the winds are slightly west of southwesterly in the Arabian Sea grid and exactly southwesterly in the Bay of Bengal grid. It also revealed that the winds are relatively steady in the latter case. Such distribution also gave an idea about the period of occurrence for a given *u* and *v* component of wind in a month, which were utilized to derive probable wind variations.

In a given month, for any particular region in the Arabian Sea or the Bay of Bengal, wind variations can take place in a variety of ways and it is very difficult to determine the winds during extreme weather conditions such as cyclones and hurricanes. However, if one excludes extreme weather conditions, there are a few simple rules which may apply for the weather variations in a given area. It is very likely that strong winds blow southwesterly over long distances in the open Arabian Sea during the month of July. Irrespective of the month and region, winds of low magnitudes vary more in direction compared with winds of high magnitudes. It means that steadiness increases with increase in wind speed. Variations in wind

speed can be associated with changes in direction, which can be either clockwise or anti-clockwise. If the wind speed goes on increasing, it should start decreasing after it reaches a maximum. Likewise, there are a number of thumb rules which can be easily adopted. The present study adopts the simplest pattern of wind variation in four different phases. In the phase-I, it was considered that wind speed increased from calm to the maximum and the direction changed clockwise and in the next phase winds decreased from maximum to minimum of Phase-I. In phase-III wind speed increased from minimum of Phase-II to the maximum possible value but the direction gradually changed anti-clockwise. In the last phase, winds decreased from maximum to minimum wind value of Phase-III. The wind variations from Phase-I to IV fairly represented the mean climatic year of wind for the respective grid areas.

In a given month, a particular *u* and *v* component of wind persist for a duration which is directly proportional to the probability density. Hence, following the above procedure, winds were estimated for all the required grids based on the probability distributions for January through December. As the probability distributions were computed based on the ten years of data from IMD, the estimated winds for establishment of mean climatic year were corrected using the sixty-year mean wind fields shown in Figure 3 for two representative months. The correction was made by multiplying the *u* and *v* components of wind uniformly by a correction factor (*F*) as indicated below:

$$F = \frac{\bar{X}_{60}}{\bar{X}_{umcy}} \tag{5}$$

\bar{X}_{umcy} is the uncorrected mean climatic year of wind. Corrected winds for the mean climatic year are shown in Figures 8a & 8b for two selected grids. Each of these figures consists of twelve stick plots representing the gross specification of the temporal wind variation from January to December.

Plot for each month contains 144 representative wind sticks that are equally spaced in time. Figures 8a & 8b give an idea on the general wind pattern for all the months in a year for the two selected grids. As the winds were estimated for all the grids, there are equivalent representative wind fields available for a given month. These winds were used as input to drive the wave model. Based on the wind input time step, the number of wind fields could vary accordingly. In this study, the wind input was provided to the model at half an hour intervals for the corresponding month as the model had provision to interpolate winds between two input fields. However, there was no restriction that only 144 wind fields were to be used as input, as stated above.

The input wind specifications to the wave model (e.g., Figures 8a & b) clearly demonstrated the most general pattern of wind variations during different months of the estimated climatic year of winds. They reflect the seasonal reversal of winds between the boreal winter and the boreal summer. Figure 8b show that, the winds are strong and steady during May to September but variable during March. Normally, deep depressions and cyclones occur in the Bay of Bengal during October and November. Thus, abnormally strong winds lasting for about a week or more would be noticed during October (Figure 8b). By and large, these winds estimated using the statistical and probabilistic approaches followed the general patterns of wind variations during an annual cycle and the same were utilized for the present simulation experiment as explained before.

4. Simulation of Wave Climate

Simulation is the process of designing a model of the real world system by conducting experiments for the purpose of understanding the system behavior, and evaluating various strategies within the boundary conditions that are imposed for executing the modelled system. In fact, real world systems are often complex and composed of several subsystems and their interactive components. The same is the case with the evolution of wind-induced surface gravity waves in the ocean. In this study, a well-established wave model was adopted. Although, the model represents the physics of the wave evolution in accordance with our knowledge today, there could be a number of potentially important effects which were not included in this version of model. Air-sea temperature differences, particularly under highly stable situations modify the energy input from the wind^[16]. The effect of rain may be significant in certain circumstances. The most trivial effect is the attenuation produced in a heavy downpour resulting in the disappearance of short gravity waves. The attenuation coefficient is the product of rain fall rate and the wave number^[17]. In addition, rain may also modify the effective mean wind profile. These are some of the examples which are to be considered in the wave prediction models used for operational wave forecasting purposes. In the present study, the above mentioned effects were less important as it dealt with the problem of wave climate simulation based on the mean climatic year of winds derived using long-term historical data. The main interest was to estimate monthly and seasonal variability of the sea-state for the region of interest.

5. Wave Model Implementation

As explained before, the wave model used was

3g-WAM^[9] originally developed at Max-Plank-Institut für Meteorologie in Humburg, Germany by S. Hasselmann with the help of P. Janssen, G. Komen, L. Zambreski and H. Gunther^[18]. The model (WAM, Cycle-4) was initially installed over 35 institutions worldwide. Naval Physical and Oceanographic Laboratory (NPOL) was one of the users of this model. The model code was originally designed for the CRAY supercomputer with UNICOS operating system which was suitably modified at NPOL for WINDOWS platforms to be used by a desk-top computer primarily for R&D applications. Incidentally, this was the first attempt to implement 3g-WAM for the Indian Seas^[19].

5.1 Regional Grid System

In this study, 3g-WAM was implemented for wave climate simulation in the Indian Seas (0-25° N, 50-100° E). The regional grid system for this region is shown in Figure 9. The land grids are indicated with solid squares. It may be noted that the regional grid system as shown in Figure 9 has only one open sea boundary to its south (0° Latitude) and there are a few sea grids to its west. Most of the wave energy that may propagate out or into the area under study is only across the southern boundary. However, both the southern and western boundaries of the grid system were extended up to 10° S and 40° W respectively to take care of swell energy advection. The sea grids and the open sea boundary grids are indicated with plus (+) and cross (x) symbols respectively. The grids which are indicated with symbols other than “+” and “x” (plus with circle around, hollow plus, and stars) also represent open sea grids. There are 915 open sea grids out of which 570 grids belong to the Arabian Sea and the rest 345 belong to the Bay of Bengal. The total number of grids between 40° and 100° E, and 10° S and 25° N is 1540 as there are 625 additional open sea boundary grids which were considered outside the regional grid system. The mean monthly wave parameters such as wave height, period and direction (combined seas and swells) reported by IDWR (1961-70) were utilized to construct the 2d-wave spectra for the open sea boundary as explained above and those were utilized as the boundary input for a given month as per the WAM convention of wave spectral input (assumed constant during a given month) for the initial warm start of the model.

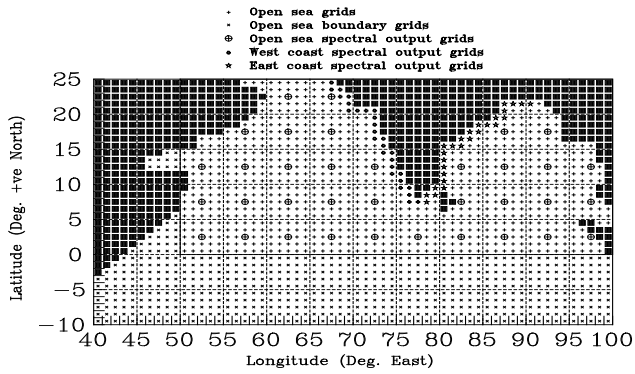


Figure 9. Wave model grid system for the Indian Seas.

5.2 Input and Output Specifications

The input data which were provided to the wave model were the estimated mean climatic year of winds and the mean monthly surface currents as discussed earlier. Figures 3 and 5 show the mean monthly wind and surface current fields only for the region between 0° and 25° N latitudes and 50° and 100° E longitudes. Data were also available/used for the open sea boundary grids shown in Figure 9. The mean monthly surface current data were supplied to the wave model at each grid point for all the model grids only once for a representative month. However, the estimated mean climatic year of winds were provided at each input time step for all the grid points of the regional grid system but the open sea boundary grids were provided with only the sixty-year mean monthly values [12].

All the gridded outputs of the model were stored at the end of each input time step while the spectral outputs were stored only for selected grids. The central grids of each 5x5 square boxes in the regional grid system are indicated in Figure 9 with the plus symbols (+) enclosed in a circle. These grids were the open sea spectral output grids. Spectral outputs were also stored for all the sea grids along the west and east coasts of India (shown with hollow plus symbols and stars respectively). There were a total of 90 spectral output grids, 35 in the open sea, 28 along the west coast, and 27 along the east coast of India.

5.3 Wave Model Execution

This simulation experiment was carried out for deep waters with current refraction. The main idea behind this study was the establishment of the climatic wave variability in terms of monthly and seasonal distributions. The mean monthly surface currents were considered as inputs which did not change during model execution for a given month as indicated above. Similarly, mean monthly winds and monthly mean wave spectra as mentioned earlier were used as inputs for the open sea boundary grids to cater for

wave propagation across the southern open sea boundaries (including few grids along western and eastern boundaries of the model grid system). It may be noted that, for the said wind and spectral inputs at the model boundaries, waves propagating into the regional grid system during the simulation were able to attain fully developed condition within the extended open sea boundary region which spans over 1000 km bordering the southern and the western boundaries of study area (North Indian Ocean, NIO or Indian Seas). These were important aspects which were essentially required for the gross specification of the associated issues in simulating the mean monthly wave conditions while dealing with the model executions over a regional grid system from the climatic point of view. However, the above boundary conditions assumed in the present study did not appear to be a limiting factor for the simulation of wave climate based on the mean climatic year of winds through temporal interpolation.

Interestingly, the simulation experiment was carried out for the full climatic year of winds by executing the model for the inputs covering the twelve calendar months of the year or 365 days. However, computer time could be saved significantly by reducing the duration of wind input appropriately from January to December. In doing so, care had been taken to achieve the desired level of accuracy for the simulated outputs. This means that the winds that are shown in Figure 8a for one particular grid in the month of January were considered as the winds that had varied for that month.

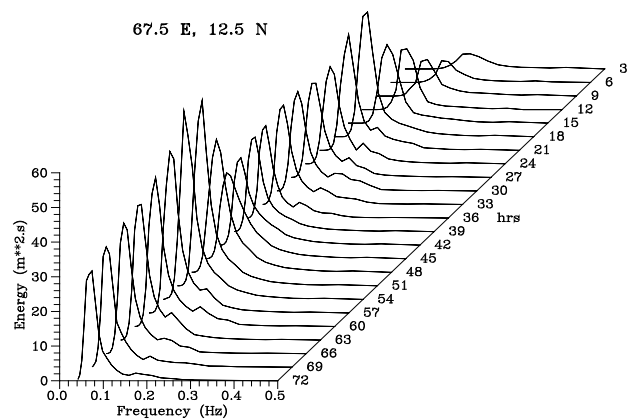


Figure 10. Evolution of wave spectrum for 72 hours of model run using estimated mean climatic year of winds for the month of July.

The model run representing a month was found to be very appropriate in this simulation experiment which reduced computation times considerably and the swell waves generated at the extended boundary region were able to reach the coastal grids of east and west coast of

India. First of all, the estimated mean climatic year of winds which were to be used as inputs to the wave model allowed the waves to grow and decay in four phases so that it could satisfy the most general patterns of wind and wave variabilities often encountered in the field. During the first phase, with the increase of wind speed, waves were allowed to grow from initial sea-state (warm start) or the wave spectral equivalent of the initial wind field. It was evident that, the waves started to decay during the second phase as the winds gradually decreased next to it. Towards the end of the decay phase, the winds again increase gradually (Phase-III) resulting in further growth of waves. During the last phase, waves again decayed gradually with the withdrawal of wind. These are the four stages through which growth and decay of waves were taken care in this study. It may be further noted that, the growth of waves during the simulation continued for the two phases. Therefore, even for a wind speed of 20 m/s the waves were able to attain the fully developed stage within a period of growth (increasing wind) since fetch was not a limiting factor. Similarly, the swell waves of 9 to 25 s period either in the Arabian Sea or Bay of Bengal could propagate from one end of the regional grid system to the other within 72 hours. Moreover, a wave of 5s period could also propagate over 2000 km. Hence, a minimum of 72 hours model run could satisfy the requirement of propagation of waves from the other generating areas within the Arabian Sea and Bay of Bengal.

Model executions were carried out for all the months using wind input as discussed above for each of the twelve calendar months (total 12 model runs). The initial wave field was set to the fully developed sea following Phillip's spectrum. Normally, the initial winds are of low magnitudes. Therefore, the parameters of the wave spectrum were chosen accordingly to compute initial wave energy. The wind input, source integration, and propagation (spherical co-ordinates) time steps were set to 1800, 600, and 1800s respectively. The output time step for the integrated wave parameters for total sea and swell were set as 1800 s. The spectra of total sea and swell were stored for every 3 hours.

Figure 10 shows the evolution of the simulated wave spectrum for 72 hours of model run for one particular grid during the month of July. It is just an example and it is quite interesting to note that the spectra could gradually grow for the initial 18 hours and lead to decay for the next 18 hours. The same sequence followed for the subsequent hours. The peak of the spectrum gradually became sharper and the energy slowly got shifted to the lower frequencies. During the decrease in winds, a secondary peak developed at the high frequency region although it was not very sig-

nificant for this representative grid. By and large, Figure 10 reveals that the simulation results were in close agreement with the input winds specified to the wave model.

5.4 Compilation of Model Outputs

All the integrated wave parameters namely the significant wave height, mean wave direction, mean wave frequency, friction wind speed, friction wind direction, peak wave frequency, sea-state dependent drag coefficient, normalized wave stress, swell wave height, mean swell direction, mean sea direction, and mean swell frequency were saved for all the grids of the regional grid system at every 30 minute intervals. A complete analysis of all these parameters would not be practical in this study. Therefore, out of the twelve output parameters, only six of them namely significant wave height, significant wave period (inverse of peak wave frequency), wind sea direction (mean sea direction), swell wave height, swell wave period (inverse of mean swell frequency), and swell direction (mean swell direction) were compiled and the monthly mean fields are presented. In addition, seasonal mean output fields were estimated only for the significant parameters. The bivariate and cumulative distributions of significant wave height and period were also computed for both the rough weather (May-September) and fair weather (October-April) seasons in the Arabian Sea and Bay of Bengal.

6. Validation of Simulated Wave Climate

The most important requirement for an appropriate validation of the simulated wave climate of a region is the availability of adequate and reliable sea-state measurements. However, the present simulation experiment for the Indian Seas was carried out in spite of limited deep water wave measurements which were of short durations. Certainly, it is not possible to have a detailed validation of the simulation results with the available wave measurements. Therefore, a qualitative validation of the wave parameters was carried out using available data namely ship-borne wave recorder data in deep waters (> 30 m depth), ship-reported visually observed data and the GEOSAT altimeter data. The following sections deal with the validation of the simulated wave climate with these data sets.

6.1 Validation using Visually Observed Wave Data

In the absence of sufficient wave measurements using state-of-the-art equipment, an attempt was made to compare the simulation results with visually observed mean monthly wave parameters. Along with the wind data, the wave data used for the comparison were obtained from IMD for the same ten-year period (1961-70). The distri-

butions of wind sea and swell data for the Indian Seas are shown in Figures 11a and 11b respectively. Table 2 shows the number of wind sea and swell observations over the whole of the Arabian Sea and Bay of Bengal for different months. It may be noted that visually observed swell directions were reported to the nearest multiple of 10 degrees while there were only 12 directional bands considered for the wave model. The comparison between visually observed and simulated swell directions is not shown here.

Table 2. Number of visually observed windsea and swell observations obtained from IMD for the period 1961-70.

Sl .No.	Month	Windsea	Swell
1	January	30,414	17,525
2	February	29,966	16,609
3	March	29,005	17,245
4	April	24,767	17,829
5	May	33,988	23,086
6	June	36,683	24,894
7	July	37,253	25,617
8	August	37,596	26,163
9	September	31,266	22,243
10	October	26,978	19,574
11	November	27,576	18,258
12	December	30,523	18,139
TOTAL		3,79,015	2,47,182

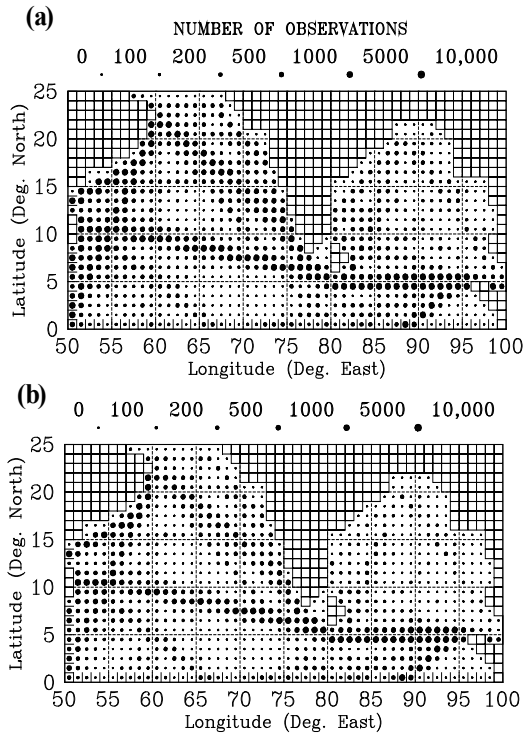


Figure 11. Visually observed [a] windsea and [b] swell data distribution (1961-70).

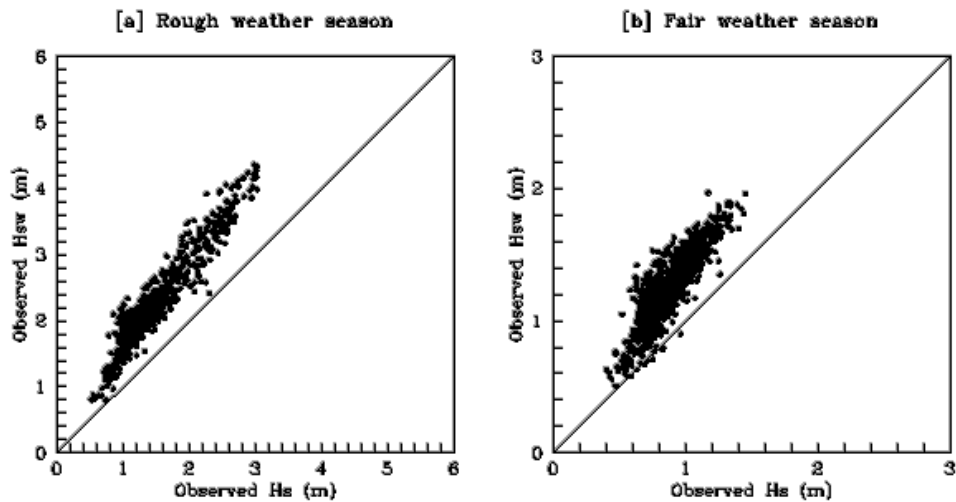


Figure 12. Scatter plot for visually observed significant wave height, and swell wave height for Indian Seas.

However, the model simulated mean monthly swell directions had general agreement with observed wind distribution, especially in the strong wind zones which generate high waves. For comparisons between the observed and simulated height and periods, the swell observations that do not have the direction information were also considered. For the comparisons between the observed and simulated wave parameters, the mean monthly fields of visually observed wind sea and swell heights were estimated over 1x1 square grids. The grids having less than 30 observations were excluded for comparison.

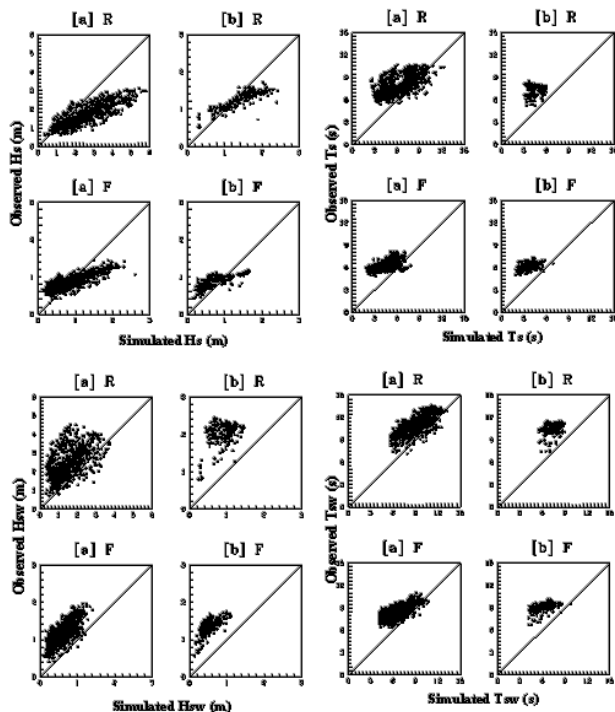


Figure 13. Comparison between simulated and visually observed Hs, Ts, Hsw, and Tsw. [a] Arabian Sea, [b] Bay of Bengal, R – rough weather, and F – fair weather.

These mean monthly fields revealed that swell wave heights reported by ships were mostly higher than windsea heights. Hence, the mean monthly windsea and swell heights for different months were grouped into rough weather and fair weather seasons and the gridded information is shown in the form of scatter plots as in Figure 12. The figure clearly indicated that swell wave heights were always higher compared to windsea heights during both the seasons. Swell heights could generally exceed windsea height under certain circumstances especially during the fair weather season. Field measurements indicated the presence of swell waves during southwest monsoon period, but their magnitudes remained less, unless the prevailing winds were relatively weak^[20]. Baba and Harish (1986)^[21] had analyzed the wave spectra collected from some lo-

cations along the southwest coast of India which revealed the presence of secondary peaks in the low frequency region. It was most likely that the mean swell heights during the rough weather season were lower than the mean windsea heights for both the Arabian Sea and Bay of Bengal. But the reverse is the case in Figure 12. Probably, it could have been difficult for a visual observer to estimate the actual swell wave height as the windseas always ride on top of the long period swells. Hence, there could be a bias during the estimation of swell heights onboard ship. It may also be noted that visually observed wave heights were reported to the nearest 0.5 m. Hence, the error in the estimation could be less for higher wave heights.

The observed versus simulated Hs for the Arabian Sea and Bay of Bengal during rough and fair weather seasons showed that the visually observed Hs were generally low compared with the simulated Hs which exceeded 1.0 m (Figure 13). One of the reasons for this may be that ships normally avoid rough weather conditions. During the fair weather season, visually observed Hs remained higher for both the Arabian Sea and Bay of Bengal compared to simulated Hs < 1.0m. The comparison between observed and simulated Ts revealed that the former was higher during rough as well as fair weather seasons in both the Arabian Sea and Bay of Bengal. Similarly, the visually observed Ts (Figure 13) varied between 4 and 11s while the simulated Ts varied from as small as 1.5 to 13 s. Moreover, the visually observed Ts supposed to be always higher than 4s as this is the minimum period reported by ships. Although visually observed swell heights (Hsw) were usually over-estimated, the observed and simulated Hsw and swell periods (Tsw) for the Arabian Sea and Bay of Bengal during rough as well as fair weather seasons (Figure 13) were compared to assess the extent of agreement between them. Observations were widely scattered during the rough weather season but there were a few observations for the Arabian Sea which compared well with one another. However, the mean deviations for all the data points considered for both the Arabian Sea and Bay of Bengal were relatively higher during the fair weather season compared to the rough weather season. The comparison of observed and simulated Ts and Tsw also showed considerable similarity. This gave an indication that observed Tsw did not indicate significant deviations compared with Hsw.

6.2 Validation using Measured Wave Data

The ship-borne wave recorder (SBWR, Model 5254, Institute of Oceanographic Sciences, UK) data for the Indian Seas covering the period 1978-93 were obtained from the Indian National Oceanographic Data Centre (IN-ODC) of NIO, Goa (presently Indian National Centre for

Ocean Information Services – INCOIS, Hyderabad is the INODC) and used for validation of the simulated wave climate. These data were collected during various oceanographic programmes. Data records of 15 minute durations were analyzed [22, 23]. Data distributions for the rough weather and fair weather seasons are shown in Figures 14a and 14b respectively. There were 785 observations during the rough weather season and 984 observations during the fair weather season for the whole of the Arabian Sea and Bay of Bengal. The digits shown are the number of observations for the respective 1 x 1 square grid. About 50 percent of the grids do not have any data. In the case of visually observed wave data, monthly means were obtained for all the grids of the regional grid system with minimum 30 observations and compared with the respective mean values by grouping them into seasons. However, the same could not be done in this case due to insufficient data. Therefore, the mean monthly Hs and Ts were computed based on the available observations for rough weather and fair weather seasons. The seasonal mean parameters were then compared with the seasonal means of simulated parameters.

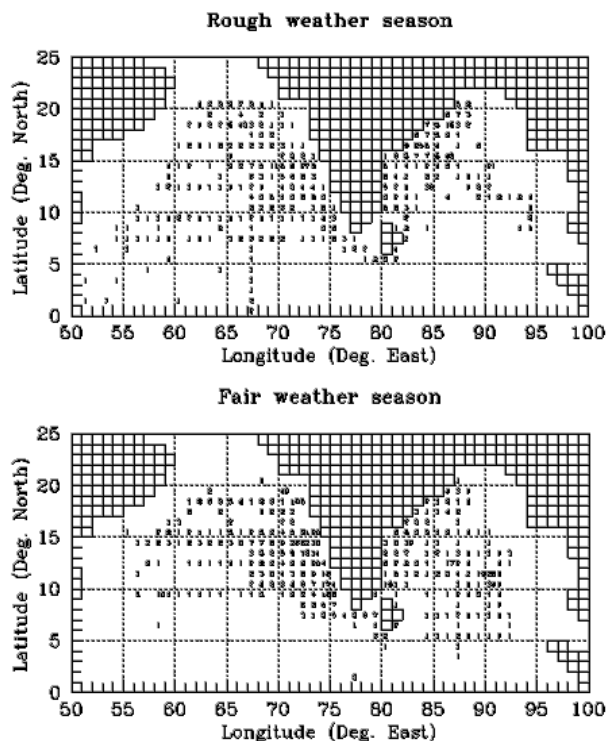


Figure 14. Shipborne wave data distribution for Indian Seas (1976-93).

The scatter between observed (SBWR) and simulated Hs and Ts for both the Arabian Sea and Bay of Bengal during rough weather and fair weather seasons are shown

in Figure 15. The observed Hs were somewhat underestimated compared with the simulated results during the rough weather season. It may be noted that, the observed data here are the point observation while the simulated outputs represent the mean climatic conditions. However, the comparison indicates the range of variability of the particular wave parameter is within the acceptable limits. The comparison for the Arabian Sea during fair weather season appeared to be better. Observed Hs in the Bay of Bengal during fair weather season varied over a wider range compared to the simulation output. Both the observed and simulated Hs during fair weather season indicated higher wave activity in the Bay of Bengal compared to the Arabian Sea. This is probably due to the frequent occurrences of deep depressions and cyclones in the Bay of Bengal during October-December. The simulated Ts were underestimated for the Arabian Sea during the rough weather season. In general, the observed Ts showed higher variability compared to the simulated Ts. The SBWR and simulated data did not show considerable agreement as compared to visual observations. One of the important reasons may be the insufficiency of the data although it covers a period of sixteen years. Secondly, as already mentioned before, the simulated outputs represent the mean variability, but the comparison definitely shows some confidence based on the acceptable range of measured values.

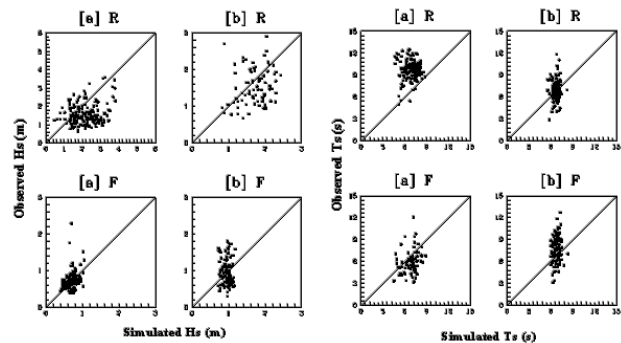


Figure 15. Comparison between simulated and measured (SBWR) Hs, and Ts. [a] Arabian Sea, [b] Bay of Bengal, R- rough weather, and F- fair weather.

Young and Holland (1996)^[24] had published the “Atlas of the oceans: wind and wave climate” based on data from the GEOSAT satellite mission. The atlas contains global and regional estimates of mean monthly wind speed, wind direction, and wave height as well as exceedance probabilities for wave heights and wind speed. Although the mean monthly fields of Hs are presented over a coarser grid resolution, they agree reasonably well with the simulated fields. The comparison between the GEOSAT and

the simulated mean monthly Hs for two selected sample sites are shown in Figure 16. The comparison is quite encouraging in the case of GEOSAT data. The reason for a good comparison could be the satellite data was available over a uniform temporal (17 day repeat cycle) and spatial resolution. The above comparison between the GEOSAT and simulated wave parameters gave a qualitative picture of the simulated waves. It also gave an idea regarding the range of wave heights and periods that were observed at different times and regions within the study area and they are well within the range of simulated results. Moreover, the comparisons are quite useful in resolving the advantages/ disadvantages of different kinds of data sets and the extent of their reliability.

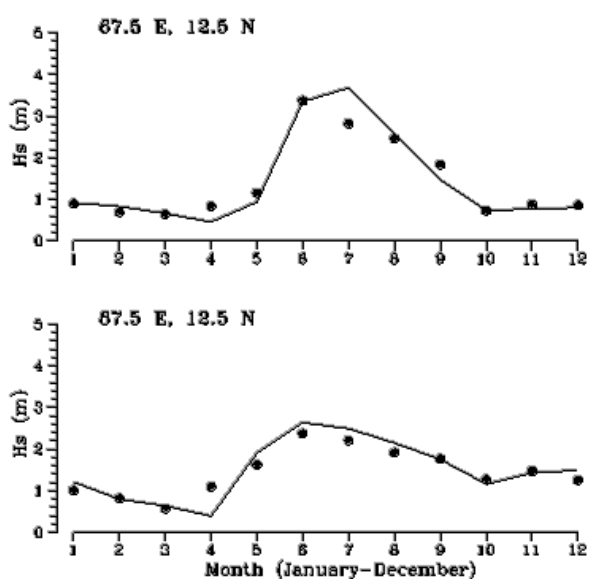


Figure 16. Comparison between simulated Hs (solid line) and GEOSAT wave height (solid circles) for two selected sites.

7. Wave Climate for the Indian Seas

The general description of wave climate of a region can be expressed in several ways. Some typical presentations are: i) monthly, seasonal and annual fields/distributions of significant wave parameters such as significant wave height (Hs) and significant wave period (Ts) or average period with or without standard deviations; ii) graphical representation of Hs and Ts in the form of histograms in several ranks and various directions similar to wind roses and iii) bivariate distributions of Hs and Ts or average period with or without classification in wave direction^[25]. From the bivariate distribution of Hs and Ts, their marginal distributions can be easily obtained. It is generally expressed in the form of percentage exceedance diagrams

or cumulative probability distributions. The wave model outputs of this simulation experiment were also compiled in the similar lines.

7.1 Spatial Distribution of Wave Parameters

The monthly, seasonal, and annual distributions of the simulated Hs and Ts in the form of contour diagrams are plotted from January through December. In addition to Hs and Ts, the monthly fields include swell wave height (Hsw), swell wave period (Tsw), windsea direction, and swell directions shown with arrows. Appropriate contour intervals were used for height (0.2, 0.3 & 0.5 m) and period (0.5 & 1.0 s) depending on the magnitude of the wave field variation in space.

7.2 Monthly Distribution

Two sample plots of mean monthly wave fields based on the present simulation study for the months of January and July are shown in Figures 17 and 18 respectively. The simulated wave fields of this study revealed significant spatial variations resulting from the combined effects of windseas generated by the local winds and swells propagating into the area of wave generation from other sources. The monthly mean variations of Hs, Ts, Hsw and Tsw for the Arabian Sea and Bay of Bengal based on the present study are given in Table 3. The height and period parameters in this table were rounded off to the nearest 0.1m and 1s respectively. Salient features for all the twelve calendar months are presented in the following sections. It may be noted that unless specified otherwise, all discussions on wave parameters hereafter refer to mean monthly values. Another important point to note is that the deep water wave measurements considered >30 m of water depth^[26] as reported in the literature are for short durations and/or not suitable/available to substantiate some of the features associated with the simulated mean monthly wave fields.

The simulated mean wave field during January as shown in Figures 17 and 18 shows considerable spatial variations of mean wave parameters from one region to another. It revealed that, during the month of January wave activity remains higher in the southwestern Arabian Sea ($H_s \cong 1.5$ m) while the north eastern region experiences low wave activity ($H_s \cong 0.5$ m). The east coast of India, the central Bay of Bengal, and the region adjacent to the southern extreme of the Indian subcontinent (Off Kanyakumari) experienced nearly 1m waves with 4 to 5s period. The general wave direction was northeasterly in January but the waves approached the west coast of India from

north to northwesterly direction. The distribution of Hsw is more or less similar to that of Hs although the magnitude is relatively less. The Hsw remained nearly the same along the west coast but along the east coast it showed a gradual increase from north to south. Swells approached the east coast from a direction around east of northeast. Ts and Tsw were higher in the southwestern Arabian Sea.

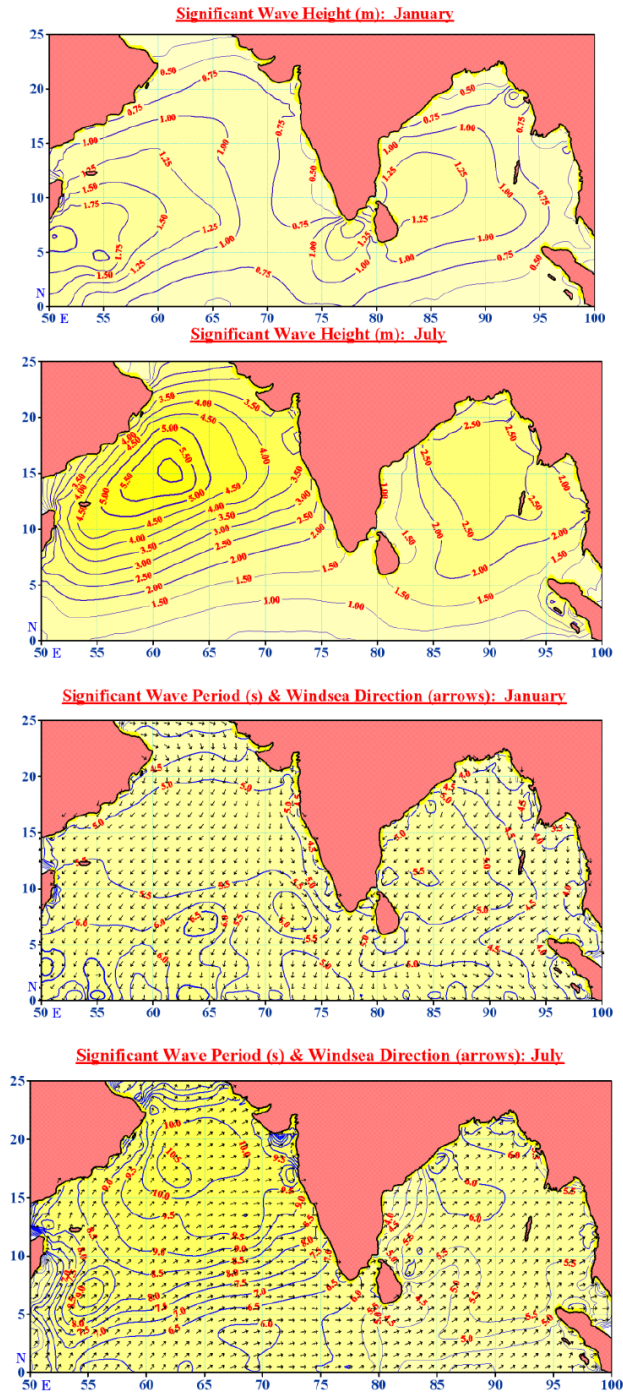


Figure 17. Distribution of significant wave height, period and windsea direction (arrows) for January and July.

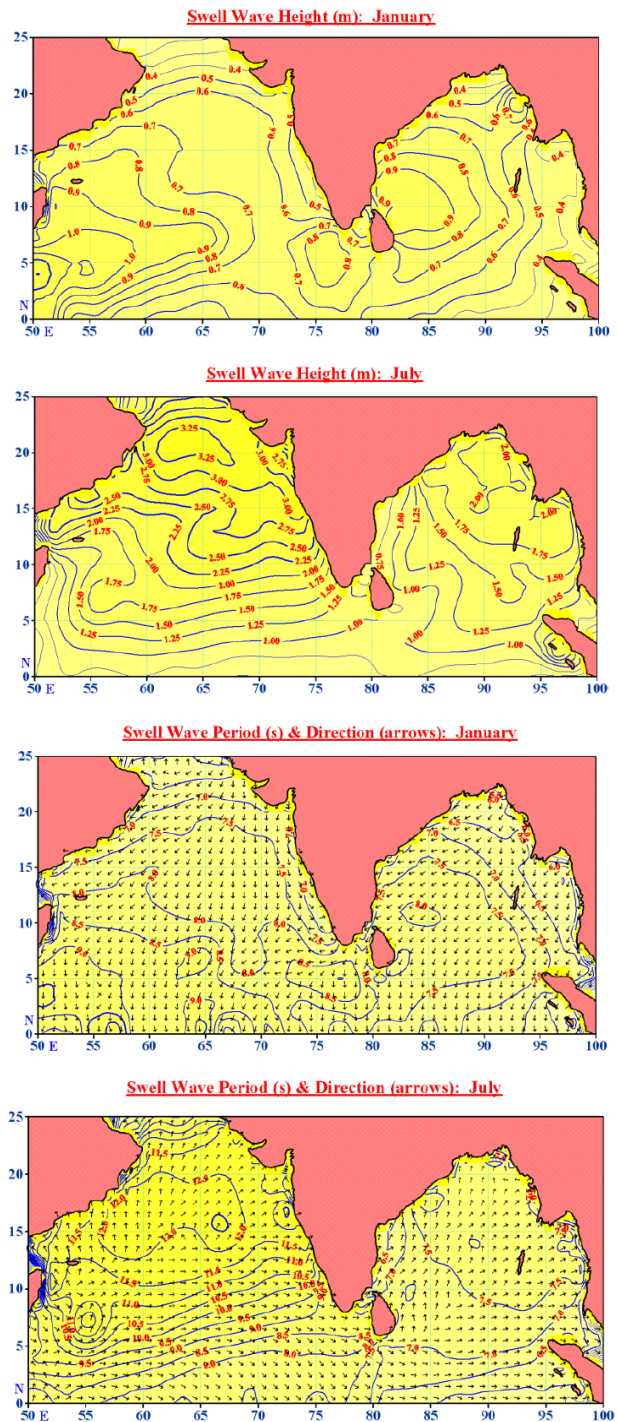


Figure 18. Distribution of swell wave height, period and direction (arrows) for January and July.

From climatic point of view, the southwest monsoon reaches its peak during July. The Indian Seas remain very rough during this month (Figures 17 & 18) compared to the rest of the rough weather months (southwest monsoon). Here, Hs varied from about 1.0 to 6.0 m in the Arabian Sea and 1 to 3 m in the Bay of Bengal. Wave directions (windsea and swell) were more or less the same

Table 3. Monthly wave height and period ranges for windsea and swell

Month	Arabian Sea				Bay of Bengal			
	Hs (m)	Ts (s)	Hsw (m)	Tsw (s)	Hs (m)	Ts (s)	Hsw (m)	Tsw (s)
January	0.3-2.1	3-8	0.2-1.3	6-10	0.4-1.5	3-6	0.3-1.2	5-8
February	0.2-1.6	3-7	0.2-1.1	5-9	0.2-1.0	3-5	0.2-1.0	6-8
March	0.3-1.2	2-5	0.3-0.9	4-8	0.2-0.8	2-4	0.2-0.7	4-6
April	0.2-0.9	2-5	0.2-0.8	3-6	0.3-1.1	2-5	0.3-0.9	4-7
May	0.6-2.4	3-5	0.5-1.5	5-8	0.5-2.1	3-6	0.5-1.4	5-8
June	0.7-4.1	4-9	0.6-2.3	6-11	0.5-2.7	4-7	0.5-1.9	6-9
July	0.6-6.1	5-11	0.5-3.2	7-13	0.7-3.0	4-6	0.7-2.2	6-8
August	0.5-5.2	4-9	0.4-2.6	6-12	0.4-2.4	4-6	0.5-1.3	6-9
September	0.4-2.7	3-7	0.4-1.6	6-11	0.3-2.1	3-6	0.3-1.3	7-9
October	0.5-1.2	2-5	0.2-0.7	5-7	0.4-1.5	3-5	0.4-1.1	4-7
November	0.4-1.4	3-6	0.4-0.9	5-8	0.4-1.6	2-5	0.3-1.0	5-7
December	0.4-1.9	4-6	0.3-1.1	6-9	0.3-1.7	3-6	0.4-1.1	6-9

during June and July except that the swells in the south-eastern regions of Arabian Sea turned further towards the equator. The Hsw showed a gradual increase from the southwest to northeast in the Arabian Sea. The distribution of Hsw over the Bay of Bengal is almost similar to that of Hs. It increased from south to north whereas along the southeast coast, it is nearly 1 m. The mean swell periods reached up to 12s and 7s respectively in the Arabian Sea and Bay of Bengal. In general, mean monthly wave parameters Hs, Ts, Hsw and Tsw reached their maxima during July.

7.3 Seasonal Distribution

The major source of deep water wave data is the NDBP (National Data Buoy Programme) buoy measurements of NIOT (National Institute of Ocean Technology, Chennai). There are also some shallow water measurements available at a few selected locations along the east and west coast of India and near Island stations. As the wind pattern completely reverses between the boreal winter and the boreal summer monsoons over a large part of the Indian

Ocean, the wave field over the Arabian Sea and Bay of Bengal also showed significant seasonal variations (Figure 19). The mean Hs over the Arabian Sea and Bay of Bengal during the rough weather season (May-September) reached up to 3.5 and 2.5 m respectively. The minimum Hs was around 1.0 m for the whole of Indian Seas. Hs maxima were noticed around the northwest Arabian Sea region and the central Bay of Bengal. However, during the fair weather season (October-April), the mean Hs in the Arabian Sea and Bay of Bengal reached up to 1.2 and 1.0 m respectively. The minimum Hs was as low as <0.5 m over the Arabian Sea and Bay of Bengal. The Hs maxima in the Bay of Bengal shifted towards southwest and the same is noticed in the southwest extreme of the Arabian Sea. Ts has varied from 6 to 9 and 5 to 7s respectively in the Arabian Sea and Bay of Bengal during the rough weather season while the same varied from 7 to 9 and 6 to 8s respectively during fair weather season. In general, the simulated wave heights for the rough weather season were about three times higher than those for the fair weather season.

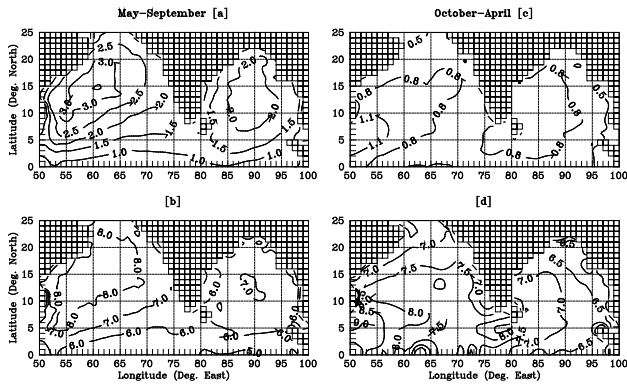


Figure 19. Distribution of significant wave height and period during rough weather (a & b) and fair weather (c & d) seasons.

7.4 Annual Distribution

Annual distributions of H_s and T_s for the Arabian Sea and Bay of Bengal are shown in Figure 20. The average H_s over the Arabian Sea and Bay of Bengal varied from about 0.7 to 2.0 and 0.6 to 1.6 m respectively. H_s maxima appeared in the western Arabian Sea (>1.8 m) towards the Arabian coast and the central Bay of Bengal (> 1.5 m). Average H_s in the south west coast is 1m which had increased gradually towards north west coast. Average T_s varies from 5 to 8s for the Arabian Sea and Bay of Bengal. The T_s maxima followed the wave height distribution to a considerable extent.

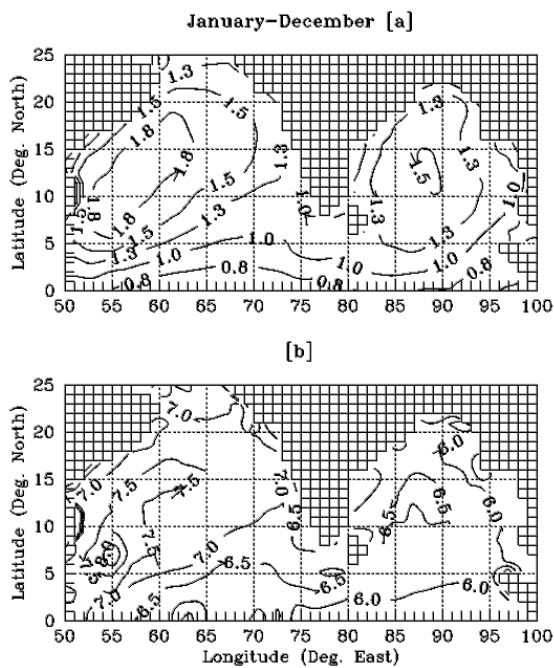


Figure 20. Annual distribution of [a] significant wave height and [b] period.

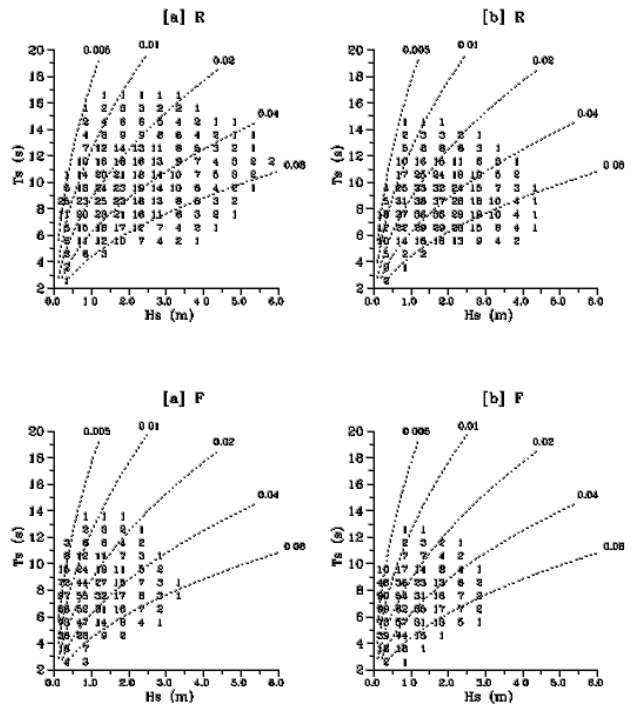


Figure 21. Bivariate distribution for H_s and T_s . [a] Arabian Sea, [b] Bay of Bengal, R – rough weather and F – fair weather.

7.5 Statistical Distribution of Wave Height and Period

In this study, the monthly distributions of wave height and period for the different regions in the Arabian Sea and Bay of Bengal were not attempted. However, seasonal distributions of H_s and T_s for both the Arabian Sea and Bay of Bengal were brought out for both the rough weather and fair weather seasons.

7.6 Bivariate Distribution

The bivariate distributions of H_s and T_s gave a detailed information on wave climate of a region. Figure 21 presents the number of occurrences out of 1000 for the respective wave heights (H_s at 0.5 m interval) and periods (T_s at 1s interval) bands during the rough and fair weather seasons in the Arabian Sea and Bay of Bengal. Dotted lines in the figure show the significant wave steepness. The correlation between H_s and T_s was found to be insignificant for all the four cases as the wave climate in the Indian Seas is composed of windseas and swells. The correlation between H_s and T_s can be significant if the wave climate is dominated by local wind waves. This is true in the case of enclosed water bodies^[25]. Figure 21 revealed that, during fair weather season there was more number of waves occurring with relatively higher period compared

to their height. It indicates that, the sea-state during the fair weather is generally dominated by swells. The H_s and T_s vary from 0.3 to 6.0 m and 3 to 17s respectively for the Arabian Sea during the rough weather season. The wave activity drastically reduced during the fair weather period. H_s and T_s ranged from 0.2 to 3.5 m and 2 to 14s respectively during the fair weather season. Similarly, in the Bay of Bengal during the rough weather season, H_s and T_s varied from 0.3 to 4.5 m and 3 to 15s respectively. During the fair weather season, they varied from 0.2 to 3.0 m and 2 to 13 m respectively.

7.7 Cumulative Distribution

Figure 22 presents cumulative distributions of H_s and T_s respectively for the Arabian Sea and Bay of Bengal during the rough and fair weather seasons. It may be noted that, the sea remained calm ($H_s < 0.5$ m) only for 5% of the time during the rough weather season. During the fair weather period the sea remained calm for about 20% of the time. The H_s exceeds 1 m for 70% of the time in both the Arabian Sea and Bay of Bengal during the rough weather season. During this period H_s exceeds 3 m for 10% of the time in the Arabian Sea and 4% of the time in the Bay of Bengal, which naturally do not include extreme weather events such as deep depressions and cyclones.

As per the cumulative distribution, H_s exceed 1m for 40% and 30% of the time in the Arabian Sea and Bay of Bengal respectively during fair weather season. During this period H_s exceeds 2 m for about 3% of the time in both these Seas. During the rough weather season T_s exceeds 5s over 95% of the time in the Indian Seas. During

fair weather it exceeds for 80% and 70% of the time in the Arabian Sea and Bay of Bengal respectively. T_s exceeds 9s for 65% and 50% of the time in the Arabian Sea and Bay of Bengal respectively in rough weather season. It exceeds the same value only for 30% and 20% of the time respectively in the Arabian Sea and Bay of Bengal during fair weather season. Only in the Arabian Sea during rough weather, T_s exceeds 15s for 20% of the time.

7.8 Spectral Characteristics

During the rough weather period the spectra were single peaked with minimum directional spread. The peak frequency and direction were 0.1 Hz and 270 respectively. Wave directions varied from around 210 to 360. On the other hand, the simulated spectra during the fair weather season showed multiple peaks and the energy spreads over various directions. The peak frequency and direction were 0.14 Hz and 330 respectively. The total wave energy during rough weather was about four times higher than that during fair weather season for the areas/locations of high wave activity. This gave an indication that the simulated spectral characteristics can be studied in detail and compared with available data gathered during field measurements in deep waters, which was not attempted in this study.

8. A Comparative Study of Wave Climate

The prevailing wind and wave conditions in the Arabian Sea and Bay of Bengal show significant differences. Most of them were already brought out earlier in this pa-

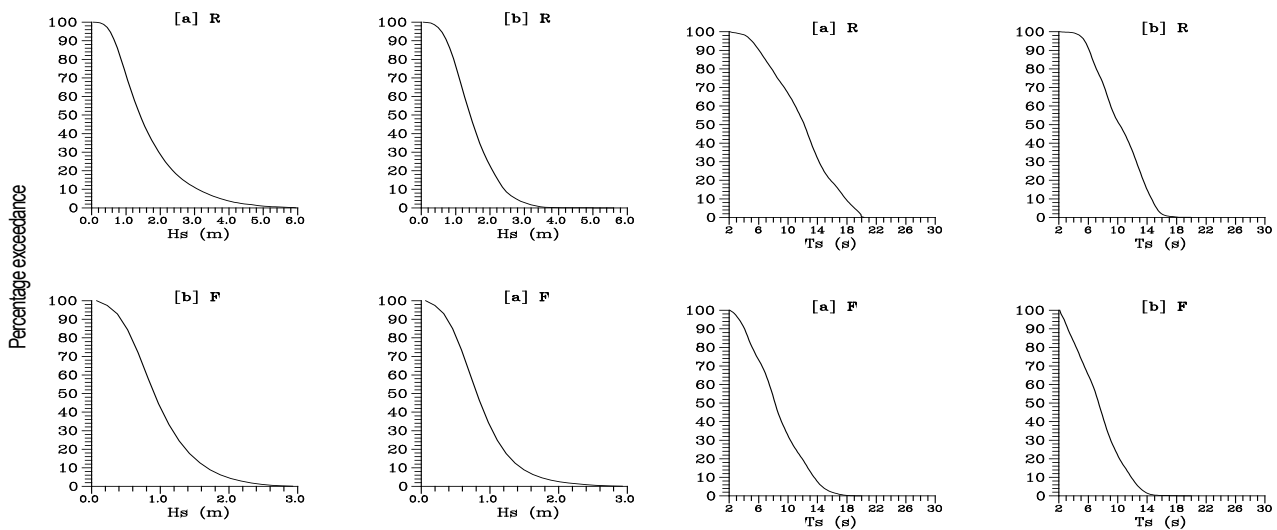


Figure 22. Cumulative distributions for H_s and T_s . [a] Arabian Sea, [b] Bay of Bengal, R – rough weather and F – fair weather.

per. A few other important features are brought out in the following sections:

8.1 Arabian Sea and Bay of Bengal

The area of the Bay of Bengal is about 60% of the Arabian Sea. Although, most of the cyclone activities are in the Bay of Bengal, the annual mean wind field over the Arabian Sea is stronger than that of Bay of Bengal. Therefore, the annual mean wave field showed higher Hs and Ts which prevailed in the Arabian Sea. However, the average Hs over the Arabian Sea and Bay of Bengal during the fair weather period remained nearly the same but the Ts was higher in the Arabian Sea. During rough weather season the wave activity was higher (Hs and Ts) in the Arabian Sea compared with the Bay of Bengal. Higher waves were generally noticed towards the western Arabian Sea and the western Bay of Bengal during November to March. During October, the southern Arabian Sea and the Bay of Bengal remained rough while the northern parts were rough during April. The general wave direction (mean windsea and swell) was northeast during November to February and southwest during May to September. However, during May-September waves moved towards east from the central Arabian Sea and appeared to propagate towards the west coast of India. Significant changes in wave direction were observed from February to March and April to May. Similar changes were also observed during the transition months of October-November.

8.2 East and West Coasts of India

There were remarkable differences between deep water wave conditions along the east and west coast of India which is mainly governed by the prevailing wind conditions and the advection of swell from other areas of wave generation. During the rough weather season (May to September), Hs and Ts gradually increased from south to north along the west coast (Figure 19). There was marginal increase in Hs and Ts from south to north along the east coast. By and large, wave activity was relatively high along the west coast compared to east coast. However, the reverse was the case during fair weather season which is seen from the monthly and seasonal distributions. Hs and Ts increased from north to south along the east coast of India except during the month of April. However, these parameters remained more or less constant along the west coast. Wave directions along the east and west coast of India also showed remarkable differences. During the rough weather season waves off the east coast were from south to southwesterly direction. On the other hand, the waves approached the west coast from directions which

vary from southwest to north of northwest. The general wave direction along the west coast of India was around northwest during fair weather season. Along the east coast, the wave direction was around northeast during November-January. Wave directions varied along the coast for the rest of the period during fair weather season (October-April).

8.3 Limitations of Simulated Wave Climate

The present simulation experiment cannot replace the hindcast wave climate although care has been taken to predict wave variability in terms of mean monthly fields of significant wave parameters. Ideally, wave climate based on long-term wave measurements using standard equipment is superior to all other methods of wave climate estimation. It may be possible to utilize measured data for this purpose at some specific sites of interest but not over very large areas such as the Arabian Sea and Bay of Bengal. A most promising method is the satellite remote sensing, which provides large coverage of the ocean surface. SAR (Synthetic Aperture Radar) provides direct measurement of two-dimensional wave spectra. For example, Young and Holland (1996)^[24] have published “the atlas of the oceans: Wind and wave climate” based on GEOSAT altimeter data (4 x 4 resolution) covering about 3 and a half years. However, the average data density for each grid (4 x 4 degrees) in this atlas varies from about 17 to a maximum of 32 per month. Satellite data with higher/desirable accuracy over several years shall provide a long-term wave climate for the specific regions of interest which can be established over a finer grid resolution.

In this study, the basic wind data utilized for the establishment of a mean climatic year of winds were reported by ships of opportunity. Ship reported data are mostly restricted to shipping routes. Hence, data density was low for the rest of the areas. Also ships have the tendency to avoid rough weather. Therefore, ship-reported wind data do not include such observations which are considerably higher compared to those under normal wind conditions although they occur less frequently. The basic wind data of IMD for a ten-year period was utilized here for the estimation of probability density for a given u and v component of wind. The same was combined with the sixty-year mean monthly wind fields of Hastenrath and Lamb (1979)^[12] for deriving a “mean climatic year of wind”. Naturally, confidence limits for the estimated mean climatic year of winds would have improved if the basic wind data were available for more number of years.

9. Conclusions

The importance of this study was that, the third generation wave model WAM utilized a “mean climatic year of winds” estimated using limited historical wind measurements. The mean climatic year of winds for the study region (Indian Seas) was prepared following the statistical and probabilistic approaches as the winds considered were widely scattered in space and time. The study could reveal that the results of the wave climate simulation were promising. Therefore, this is an useful demonstration for conducting such simulation experiments in the areas where wind as well as wave measurements are the limiting factor. The second important aspect of this study is that it could minimize the computing time and associated resources. The climatic database obtained from such simulation experiments can be put to use for several practical applications. They can be a useful to all those who are concerned with coastal and offshore activities. Moreover, site specific wave climate at selected locations can also be met by making use of the simulated database.

Acknowledgement

The first author would like to express sincere thanks to The Director, NPOL for providing the facilities required for this work. This study was part of his Ph.D. under CUSAT, Cochin, India. The wind, wave and surface current data used in this study were obtained from various sources. The authors are grateful to all the heads of the institutes concerned who had supplied the necessary data to undertake this work.

References

- [1] Cavaleri, L. et. al., (The Wise Group), 2007, “Wave modelling – the state of the art,” *Prog. Oceanogr.*, 75, pp. 603-674.
- [2] Liu, P. C., Schwab, D. J., & Jensen, R. E., 2002, “Has Wind-Wave Modelling reached its limit?,” *Ocean Eng.*, 29, 81-98.
- [3] Cavaleri, L., 2009, “Wave Modeling – Missing the Peaks,” *J. Phys.Oceanogr.*, 39, 2757-2778.
- [4] Cavaleri, L., 2006, “Wave Modelling – Where to Go in the Future,” *Bull. Amer. Meteor. Soc.*,” 207-214.
- [5] Swain, J., Umesh, P. A., and Harikrishnan, M., 2010, “Role of Oceanography in Naval Defense,” *Ind. J. of Geo-Mar. Sci.*, 39, pp. 631-645.
- [6] Janssen, P. A. E. M., 2008, “Progress in Ocean Wave Forecasting,” *J. Comp. Phys.*, 227, 3572-3594.
- [7] Raj, Kumar., et al., 2009, “Improvement in predictability of waves over the Indian Ocean,” *Nat. Haz.*, 49, pp. 275-291.
- [8] Bishop, C. T., and Donelan, M. A., 1989, Wave prediction models, *Applications in Coastal Modelling*, Elsevier Oceanography Series, Edited by V C Lakhan and A S Trenhaile.
- [9] Hasselmann, S., et al., 1988, “The WAM-Development and Implementation Group (WAMDI). The WAM Model - A third generation ocean wave prediction model,” *J. Phy. Oceanogr.*, 18, pp. 1775-1810.
- [10] Komen, G. J., et al., 1994, *Dynamics and Modelling of Ocean Waves*, Cambridge, UK: Cambridge University Press.
- [11] Vihang, Bhatt., et. al., 2004, “Impact of Oceansat-I MSMR data on analyzed oceanic winds and wave predictions,” *Ocean Eng.*, 31, pp. 2283-2294.
- [12] Hastenrath, S., and Lamb, P. J., 1979, *Climatic atlas of the Indian Ocean, Part-I, Surface Climate and atmospheric circulation*, The University of Wisconsin Press, USA.
- [13] Mathews, J. H., 1987, *Numerical methods for Computer Science, Engineering and Mathematics*, Prentice-Hall International, London.
- [14] Carnahan, B., Luther, H. A., and Wilkes, J. O., 1969, *Applied numerical methods*, John Wiley & Sons, INC, New York, USA.
- [15] Jenkins, G. M., and Watts, D. G., 1968, *Spectral analysis and its applications*, Holden-day, Oakland, USA.
- [16] Cardone, V. J., 1969, *Specification of the wind distribution in the marine boundary layer for wave forecasting*, Geophysical Science Laboratory, TR-69-1, School of Engineering and Sciences, New York University.
- [17] Phillips, O. M., 1987, “Ocean-wave prediction, where are we?,” *Johns Hopkins APL, Technical Digest*, Vol. 8, pp. 7-10.
- [18] Gunther, H., Hasselmann, S., and Jansen, P. A. E. M., 1992, *Wamodel, Cycle-4 (Revised Version)*, Technical Report No.4, Dautches KlimaRechenZentrum, Hamburg.
- [19] Swain, J., Ananth, P. N., and Prasada, Rao, C. V. K., 1995, *Test results of the third generation wave model for fetch and duration limited wave growth*, Departmental Research Report, No RR-7/95, NPOL, Cochin, India.
- [20] Swain, J., 1992, “Application of Kruseman’s mean wind wave spectrum for sea-state composition,” *Ind. J. of Mar. Sci.*, 21, pp. 89-98.
- [21] Baba, M., and Harish, C. M., 1986, “Wave height and period distribution along the southwest coast of India,” *Ind. J. of Mar. Sci.*, 14, pp. 1-14.
- [22] Tucker, M. J., 1963, *Analysis of records of sea waves*, *Proceedings Institution of Civil Engineers*,

- London, UK, pp. 305-316.
- [23] Draper, L., and Tucker, M. J., 1971, Determination of wave conditions for Marine Engineering, Dynamic waves in Ocean Engineering, Wiley-Interscience, pp. 389-402.
- [24] Young, I. R., and Holland, G. J., 1996, Atlas of the Oceans: Wind and Wave Climate, Pergamon, Elsevier Science, USA.
- [25] Goda, Y., 1990, Distribution of sea state parameters and data fitting, Wave phenomena and coastal structures, Hand book of Coastal and Ocean Engineering, Gulf Publishing Company, London, Vol.1, pp. 373-408.
- [26] Michael, Clancy, R., and Johnson, A., 1997, "An overview of naval operational ocean modeling," Mar. Tech. Soc. J., 31, pp. 54-62.